J. Eng. Technol. Sci., Vol. 53, No. 4, 2021, 210405

An Analytical and Experimental Evaluation of a Heat Sink under Constant Heat Flow and Forced Convection Heat Transfer

Ehsan Fadhil Abbas

Kirkuk Technical College/Northern Technical University, Kirkuk, Iraq
E-mail: ehsanfadhil@ntu.edu.iq

Highlights:

- Experimental experiments were performed on a straight finned heat sink at constant heat flux and variable volume airflow rate.
- The experimental result was examined by using the 1D-transient exact solution equation on the fin.
- The temperature distribution across the fin and the heat dissipation were investigated.
- The result of the comparison showed a good agreement between the exact solution and the experimental result.

Abstract. In this study, the exact transient differential equation was used to calculate the convection heat loss in a heat sink with a rectangular cross section fin. The result of the analytic solution was compared to the result from experiments conducted on a standard heat sink. The experiments were performed at a constant heat flow of 9000 W/m^2 and a low airflow rate ranging from 12 to 100 cm^3/s in seven steps. The comparative results showed that while there was good agreement between the experimental result and the exact solution, the average error ratio increased with an increase of the airflow rate. However, the maximum average error ratio between the experimental result and the exact solution did not exceed 6.4%. The maximum temperature distribution in the heat sink was obtained at a time of 900 s in all experiments.

Keywords: *fin simulation; flat fin array; heat loss by fin; heat sink; transient solution.*

1 Introduction

The extended surfaces of a heat transfer exchanger device have fins connected to its primary surface. Fins are used to improve the heat transfer performance of thermal engineering equipment by increasing the heat exchange surface. They can be designed with different geometries, such as pins, flat or corrugated plates, and brush wires that may be made with regular or irregular cross-sections. Fins are most commonly used in thermal units such as heat exchangers, electronic heat sinks, electric machines, power plants, and petrochemical units. Given the importance of heat exchangers in industrial plants, many researchers have

Received July 8th, 2020, Revised ,September 21st, 2020 Accepted for publication April 22nd, 2021.
 ISSN: 2337-5779,
DOI: 10.5614/j.eng.technol.sci.2021.53.4.5

conducted theoretical and experimental studies on heat exchangers to improve their efficiency using an extended surface.

A number of theses studies have focused on design optimization of a flat-plate heat sink. Yen & Chang [1] optimized the longitudinal fin array in a forced convection system, considering different profile areas, such as triangular, rectangular, concave parabolic, and convex-parabolic profile areas. Optimization of aspect ratio, inter-fin spacing, and heat transfer properties has been investigated with specific engineering of the base plate, fin region, and continuous thermal conductivity. Kou, *et al*. [2] developed an analytical solution to obtain the optimum height of a heat sink, with the solution being based on the Bi number (Biot number) and the coefficient of convection heat transfer ratios. Cohen, *et al*. [3] extended the use of a least-material single rectangular plate-fin analysis to theoretically multiple fin arrays, using a composite Nusselt number correlation. The total heat removal, heat removal per unit mass, and claimed specific heat removal were obtained for various heat sink materials.

Shih & Liu [4] developed an optimized design for a plate-finned heat sink based on the systematic improvement of maximum heat removal in an electronic cooling system using the rate of entropy generation for maximum heat transfer efficiency. Chiang [5] studied optimizing the parameters of a parallel heat sink design based on the Taguchi method. The airflow rate and the maximum thermal resistance were used as the performance characteristics of the heat sink design parameters. The result of the numerical analysis showed that the optimum design parameters contributed to the improvement of the highest heat resistance by 15%. Chiang [6] investigated the influence of design factors of a parallel fin heat sink with cooling fan on its thermal performance using a methodical experimental design based on response surface methodology. Design parameters such as fin length and thickness, width space between fins, and the distance between the tips of the fins and the cooling fan were included in this study.

Kim & Mudawar [7] presented analytical models for the various shapes of micro-channel heat sinks, such as triangular, inverse trapezoidal, diamond, and rectangular shapes. Analytic solution were offered for both homogeneous heat sinks and heat sinks with ideal insulated cover plates. The researchers found that theoretical models are very useful tools for designing and predicting the thermal performance of microchannel heat sinks in electronic cooling applications. Ventola, *et al*. [8] investigated the advantages of micro-channel grossness on enhancing the heat transfer of a heat sink cooled by forced convection. They carried out experiments on heat sinks with the surface roughness ranging from 1 to 25 μm and the Reynolds number ranging from 3000 to 17000. The results of the investigation showed that the surface roughness increased the efficiency of the heat sink by 15% compared to a standard heat sink. Raut & Kothavale [9]

investigated the influence of various properties of a heat sink fin array on its thermal performance under natural convection heat transfer, like fin thickness, fin height, and fin spacing. They found that the thermal performance of the fin array is directly proportional to the fin spacing and inversely to the fin thickness. Wu, *et al*. [10] studied a practical model to predict the hydraulic and thermal performance of a flat-plate fin heat sink for a wide range of $Re \leq 5000$. The results showed an improvement in the geometry of the current work when the pressure drop was limited to 10 mmAq and the length of the fin to 24 mm.

Next are papers that reported studies on heat and flow characteristics with partial heating in the heat sink [11-13]. Lelea [11] studied a numerical model of heat removal and flow in a microchannel heat sink with partial heating. The effect of the heating site on thermal and hydrodynamic behavior was analyzed. The results showed that the partial heating process along with the variable viscosity had a strong influence on the thermal properties and flow properties. Yoon, *et al.* [12] presented a numerical simulation of the partial heating location on the efficiency of a heat sink under forced convection. The optimal partial heating location was evaluated according to several parameters, namely heat transfer, velocity, the thermal conductivity of the heat sink, the ratio of total length to heated surface width, and the thickness of the heat sink base. Based on the simulation result, the researchers suggested that specifying the correlation of the partial heating position helps to obtain maximum thermal performance.

Lee, *et al*. [13] performed an experimental research on a partially heated basin using forced convection. They studied several design parameters, namely the effect of length and location of heating, air velocity on base temperature and efficiency. The results showed that the optimum heating location was on the upstream side in the laminar flow, unlike in heat sinks under turbulent flow. Gupta, *et al*. [14] examined the effect of dimples and protrusions on the heat and flow characteristics of a flat-plate fin array under forced convection. The Nu number and fanning friction factor were analyzed by varying two parameters, namely pitch and depth of dimples, for staggered and inline configurations. The results showed that the performance of heat transfer and flow of the fin arrays were greatly influenced by increasing the depth of the dimples.

Vinoth & Kumar [15] studied the heat and flow parameters of an inclined finned heat sink. Three different cross sections, namely trapezoidal, square, and semi-circle cross-sections, were tested using AlO_3/H_2O nano-fluid with a constant mass flow rate and variable heat flux. The experimental results indicated that the trapezoidal cross-sections performed better than the others. Rahman & Tafi [16] theoretically investigated enhanced heat transfer using a forced oscillating flat plate fin. Yu, *et al.* [17] studied heat transfer enhancement in an air-cooled heat sink using actuated plates subjected to agitation action. The numerical results

indicated that agitation increased the heat transfer rate by 61%. Sharat, *et al*. [18] looked at the effect of reducing the pressure gradient, thermal resistance, and laminar flow on the heat transfer coefficient, using various heat sinks with different cross sections, such as square, circular, and elliptical cross sections. The numerical results showed that an elliptical heat sink is the best type for electronic cooling purposes.

Duan, *et al.* [19] analyzed flow properties and pressure drop of a parallel-plate heat sink. Numerical simulation was performed on an elliptic bottom plate-fin heat sink with different inlet widths. They developed a model that can be used to predict the impact of pressure drop of fluid flow on plate-fin heat sinks. Ekpu *et al.* [20] examined the effect of heat sink geometry on the efficiency of heat sinks. The numerical results showed that the best heat removal occurred with the thinnest base and the longest fin. Teertstra, *et al.* [21] presented a model for predicting the average heat transfer rate from a plate-fin heat sink under forced convection. A simulation was done by composite solution based on the limiting cases of fully developed and developing flow between isothermal parallel plates. The resulting model had an excellent agreement over a full range of $0.1 < Ra < 100$ within a response surface methodology (RSM) difference of 2.1%.

Some of the research dealt with transient simulation of flat-fin performance [22,23]. Ma & Xu [22] numerically studied the transient flow for different heated gaps with a fin in different positions on the sidewall. The numerical result has showed there was a good match between the measuring predictions and the numerical results. Arshad, *et al*. [23] used a two-dimensional transient heat transfer simulation to simulate the heat transfer performance of a heat sink embedded in a phase change material (PCM) applied in electronic devices. The simulation was performed on two heat sinks with different thicknesses, namely 2 and 3 mm, and with power supply varying from 4 to 6 W. The numerical results showed that the utilized PCM with a low temperature maintained the heat sink base at a lower temperature. It also indicated that changing the power supply from 4 to 6 W increased the melting time by 6.36% for a 3-mm heat sink and by 1.9% for a 2-mm heat sink.

Panahizadeh [24] presented a numerical simulation on transient heat transfer for a longitudinal fin with a triangular cross-section using finite difference solved by the Fortran software. The numerical model was also examined by the CFD software to verify the result. They found that there was a good match between both results. Lakshminarasimha [25] presented a transient CFD in a simulation for fins with different cross-sections, namely tapered, round, and rectangular fins, using constant heat flux in a free convection case. The comparation results showed that the tapered fins gave a temperature distribution level that was 3% higher than that of the other fins. Naphon & Nakharintr [26] simulated the

turbulent heat transfer and flow characteristics of nanofluid streams on a mini-channel heat sink with the Reynolds number ranging from 80 to 200. They found that suspended nanoparticles give a better heat transfer improvement when compared to the result of a deionized water cooling method.

Naphon & Nakharintr [27] numerically studied the laminar heat transfer of nanofluids used as coolant in a rectangular heat sink. This study involved the application of single- and two-phase models in a 3D simulation analysis. They found that the result of the two-stage model had greater accuracy than the single-stage model in addition to the fact that the heat transfer coefficient of the nanofluids was higher than that of water. Nakharintr & Naphon [28] conducted an experimental study of the influence of a magnetic field on heat transfer characteristics and pressure drop in a rectangular heat sink. Experiments were performed using nanofluids with different concentrations of TiO nanoparticles and two different magnetic field strengths. They found that the magnetic field had a more significant effect on the Nu number compared to the non-magnetic field, while the nanofluid concentration had no significant effect on the pressure drop. Nakharintr, *et al*. [29] numerically evaluated the heat transfer and flow characteristics of nanoscale fluids in a small-channel heat sink, using an Eulerian two-phase approach. Nakharintr, *et al*. [30] practically and numerically studied the effect of the jet plate spacing to jet diameter ratios on the heat transfer and flow characteristics of nanofluids in a mini-channel heat sink. Navon, *et al.* [31] experimentally studied the effect of certain parameters on the heat transfer and flow properties of nanofluids in a mini-channel heat sink, namely nanoparticle concentrations, jet diameter, nanofluid mass flow rate, and nozzle to heat sink distance.

The aim of the present work was to compare the application of the exact transient solution of a flat-plate fin with the experimental result. The practical part included performing tests on a heat sink made of aluminum with a constant cross-section area under constant heat flux and varying airflow rates. The instantaneous heat loss from the heat sink to the airflows over it was compared with the equation of the exact transient solution of a flat-plate fin.

2 Mathematical Model

Figure 1 shows the longitudinal fin with a constant cross-section profile, assuming one-dimensional conduction convection. To determine the rate of heat loss from the fin, first of all, the equation for temperature distribution should be derived. This is determined based on the energy balance according to the law of conservation of energy on an element of the fin at location x with a thickness dx. The governing equation was simplified according to the following limiting assumptions [24,26,27]:

1. The fin has a homogeneous material and stable thermal conductivity.
2. The coefficient of heat transfer on the fin's surfaces is uniform and constant.
3. The heat loss on the lateral sides is negligible.
4. The fin's thickness is very small compared to its length and width.
5. The base fin temperature is uniform.
6. The heat transfer by radiation to surrounding fins is negligible.
7. The fin is subjected to a uniform airflow rate over its surfaces.
8. The fin does not contain an internal source for generating heat.
9. The base of the fin is perfectly joined to the prime surface and contact resistance can be neglected.
10. The amount of heat transferred from the tip, front, and back edges of the fin are very small compared to its lateral surfaces.

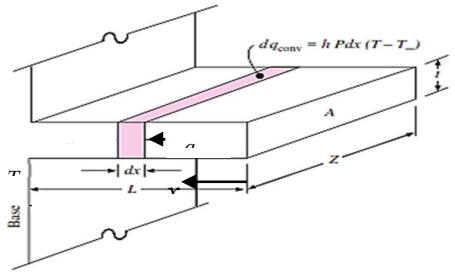

Figure 1 Sketch illustrating heat transfer through a rectangular fin [34].

$$q_x - q_{x*dx} - dq_{conv} = \dot{E} \tag{1}$$

where

$$q_x = -kA\frac{\partial T}{\partial x} \tag{2}$$

$$q_{x+d} = -kA\left(\frac{\partial T}{\partial x} + \frac{\partial^2 T}{\partial x^2}dx\right) \tag{3}$$

$$dq_{conv} = h\,P\,dx\,(T - T_\infty) \tag{4}$$

$$\dot{E} = \rho\,C\,A\,dx\frac{\partial T}{\partial t} \tag{5}$$

Substituting Eq. (2) to (5) into (1) can be rearranged as

$$\frac{\partial^2 T}{\partial x^2} - \frac{hp}{kA}(T - T_\infty) = \frac{\rho C}{k}\frac{\partial T}{\partial t} \tag{6}$$

and Eq. (6) can be solved subject to two boundary conditions

$$\frac{dT(0,\tau)}{dx} = 0 \tag{7}$$

$$k\frac{\partial T(L,\tau)}{\partial x} = q_w \ , \tag{8}$$

and initial condition

$$T(L,0) = Ti \tag{9}$$

The next step is introducing the dimensionless variables [32]:

$$\theta = \frac{k(T-T_\infty)}{q_w L} \tag{10}$$

$$X = \frac{x}{L} \tag{11}$$

$$\tau = \frac{\alpha t}{L^2} \tag{12}$$

$$N^2 = \frac{hPL^2}{kA} \tag{13}$$

Eq. (6) in dimensionless form becomes

$$\frac{\partial^2\theta}{\partial X^2} - N^2\theta = \frac{\partial\theta}{\partial\tau} \tag{14}$$

with boundary conditions

$$\frac{\partial\theta(1,\tau)}{\partial X} = 1 \tag{15}$$

and

$$\frac{\partial\theta(0,\tau)}{\partial X} = 0 \tag{16}$$

and initial condition

$$\theta(X,0) = \theta_i = \frac{k(T-T_\infty)}{q_w L} \tag{17}$$

Since Eq. (14) is nonhomogeneous, the separation variable cannot be solved directly, and the solution form can be assumed as:

$$\theta = \theta_1(X) + \theta_2(X,\tau) \tag{18}$$

Eq. (14) is split into two parts, one $\theta_1(X)$ and the other $\theta_2(X,\tau)$, as follows:

$$\frac{d^2\theta_1}{dX^2} - N^2\theta = 0 \tag{19}$$

with two boundary conditions

$$\frac{d\theta_1(1)}{dX} = 1 \tag{20}$$

$$\frac{d\theta_1(0)}{dX} = 0 \tag{21}$$

and for θ_2

$$\frac{\partial^2\theta_2}{\partial X^2} - N^2\theta_2 = \frac{\partial\theta_2}{\partial\tau} \quad (22)$$

with two boundary conditions

$$\frac{\partial\theta_2(1,\tau)}{\partial X} = 1 \quad (23)$$

$$\frac{\partial\theta_2(0,\tau)}{\partial X} = 0 \quad (24)$$

and initial condition

$$\theta_2(X,0) = \theta_i - \theta(X) \quad (25)$$

The complete solution includes the summed direct integration of Eq. (19) and the results of Eq. (22) are resolved by the separation variable method, resulting in [32]:

$$\theta = \frac{\cosh NX}{N\cos} + \left(\theta_i - \frac{1}{N^2}\right)e^{-N^2\tau} + 2\sum_{n=1}^{\infty}\frac{(-1)^{n+1}}{N^2+n^2\pi^2}\cos(n\pi)Xe^{-\left(N^2+n^2\pi^2\right)\tau} \quad (26)$$

where

$$n = 1, 2, 3, \ldots\ldots$$

The convection heat loss is calculated from the instantaneous temperature distribution via integration, expressed as follows:

$$q_{conv} = hP\int_0^L (T - T_\infty)\,dx \quad (27)$$

where

$$T - T_\infty = \frac{\theta q_w L}{k} \quad (28)$$

where $x = XL$ so that $dx = L\,dX$, if $x = 0$ $then$ $X = 0$ and $x = L$ $then$ $X = 1$

Thus

$$q_{conv} = \frac{hPq_wL^2}{k}\int_0^1 \theta\,dX \;\; = N^2 q\int_0^1 \theta\,dX \quad (29)$$

The law of conservation of energy is used to evaluate the experimental and actual heat losses from the heat sink.

$$q = \dot{m}c_p(T_{out} - T_{in}) \quad (30)$$

The result of Eq. (30) is used in Newton's law of cooling to evaluate h in order to be used in Eqs. (13) and (29). It is expressed as:

$$h = \frac{q}{PL(T-T_\infty)} \quad (31)$$

3 Experimental Work

A computer-controlled convection heat transfer unit was used in the present work to execute a practical experiment. The unit was made especially for the heat transfer laboratory as shown in Figure 1. Table 2 illustrates the resolution, accuracy and uncertainty of the measuring devices. It consisted of three parts, namely an experimental tower, a control interface box, and a PC device. The first part was made of a rectangular stainless steel rectangular duct with dimensions of 12 × 15 cm and 70 cm height. It had a square hole of 10 × 10 cm on the left side to insert the heat sink and an axial fan installed on the top end. Also, it contained eight holes on the front side for inserting type J thermocouple sensors to the working space. The experimental tower was connected to the PC device through the interface part, which worked as an intermediary between both to transfer operation orders and experimental data.

The heat sink was made of aluminum and consisted of nine flat plates perfectly jointed with the heat sink base. The dimensions of the heat sink used in the present work are illustrated in Table 1. Seven experimental tests were performed at a constant q_w of 9000 W/m^2 by changing the airflow rate from 12 to 100 cm^3/s. Uniform procedures were followed in executing the tests. First, the heat sink was heated until it reached 40 °C for half an hour at a heat flux of 1000 W/m^2 without the fan operating. The next step was setting the test rig from the PC to adjust the blower speed, heat flux, and the time for recording data, which was limited to one minute per reading. This process was repeated ten times for every airflow rate. The average values were included in the analyzed data to reduce the error percentage in the results.

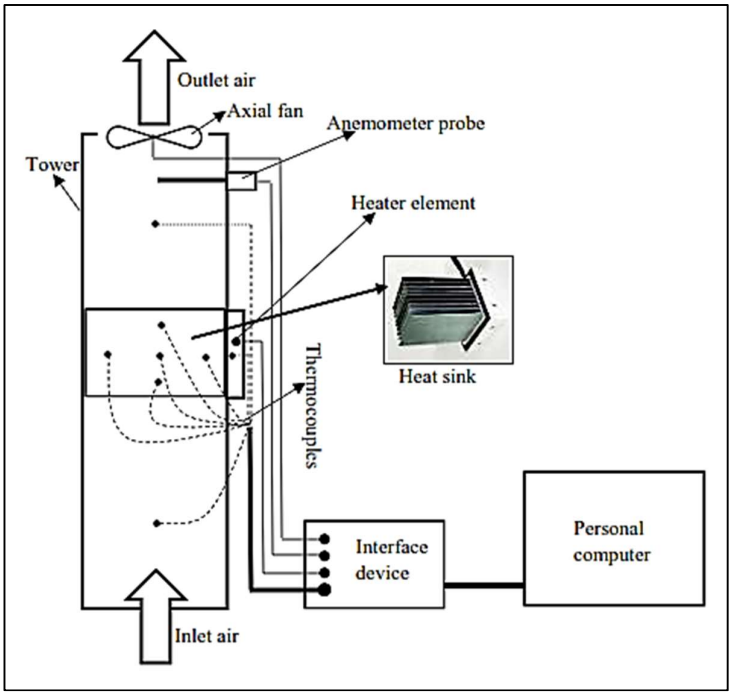

Figure 2 Schematic diagram of the test apparatus.

Table 1 Specification of the heat sink.

Part name	Dimensions
Base	Height 10 cm × width 10 cm × thick 1 cm
Fin	Length 13.5 cm × height 10 cm × thick 2 mm Number of fins: 9
Electric element	Diameter 1 cm × length 8 cm, power 150 W

4 Experimental Uncertainty Analysis

The maximum uncertainty of the heat transfer rate was calculated based on the uncertainty in the instrumentation as shown in Table 2 and the relative parameters mentioned in Eq. 31 can be expressed as follows [33]:

$$\left(\frac{\partial Q}{Q}\right) = \left[\left(\frac{U\dot{V}}{\dot{V}}\right)^2 + \left(\frac{U\rho}{\rho}\right)^2 + \left(\frac{Uc_p}{c_p}\right)^2 + \left(\frac{UT_{out}}{T_{out}}\right)^2 + \left(\frac{UT_{in}}{T_{in}}\right)^2\right]^{1/2} \quad (32)$$

The maximum uncertainty of the practical heat transfer rate in the current study was ±3.24%.

Table 2 Resolution, accuracy, and uncertainty of measuring devices.

Devices	Resolution	Accuracy	Uncertainty
Caliper	0.01 mm	±0.02	±0.156
Anemometer	0.01 m/s	±0.01	±0.215
Temperature data logger	0.1 °C	±0.2%	±0.539

5 Results and Discussion

To examine the exact transient solution of the fin with sufficient confidence for predicting the heat removal from the heat sink, validation was required. Comparisons were made between the instantaneous predicate heat removal that was evaluated by the exact solution and the experimental data obtained from the set of experiments conducted on a sample of the heat sink using a computer-controlled laboratory heat transfer apparatus. For this study to be reasonably accurate, the experiments were performed within operating conditions that were as similar as possible in terms of the experimental period, the heat flow value, and the temperature when air enters the tower. The experimental results were calculated based on the energy conservation equation, as referred to in Eq. 20. The analytic results found from the exact solution were based on the insulated tip because the ratio of the fin edge area to the total area was very small, forming only about 1.3%. Figures 3 to 8 show the operating conditions of the seven experiments conducted in this study. The supplied heat energy was 90 W, the initial conditions ranged from 23.8 to 26 °C, and the inlet air temperature entering the tower varied from 24.9 to 27.2 °C. Observed from these figures, T_b and $(T_{out} - T_{in})$ increased gradually with time and they were affected by the velocity and temperature of the airflow.

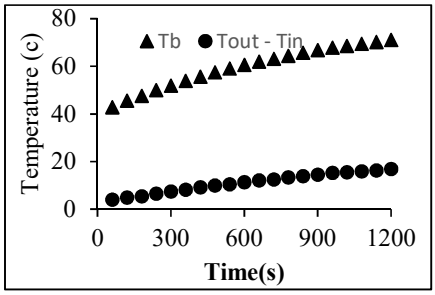

Figure 3 Temperature variation vs time when $\dot{V} = 12\ cm^3/s$.

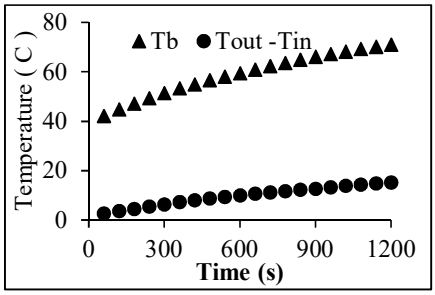

Figure 4 Temperature variation vs time when $\dot{V} = 24\ cm^3/s$.

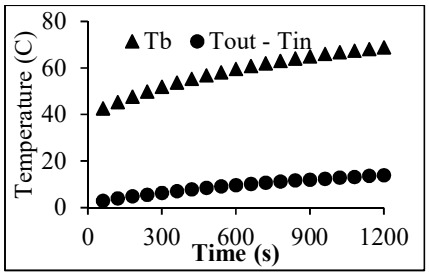

Figure 5 Temperature variation vs time when$\dot{V} = 36\ cm^3/s$.

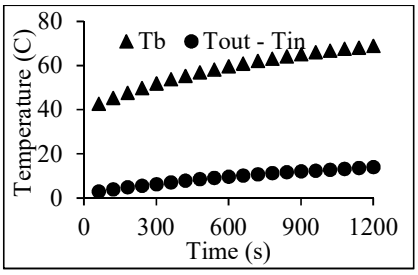

Figure 6 Temperature variation vs time when $\dot{V} = 48\ cm^3/s$.

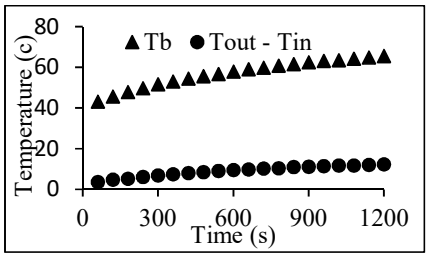

Figure 7 Temperature variation vs time when $\dot{V} = 72\ cm^3/s$.

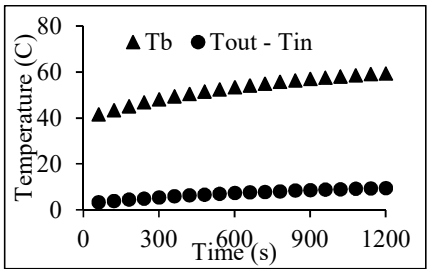

Figure 8 Temperature variation vs time when $\dot{V} = 100\ cm^3/s$.

Figure 9 shows the trend of temperature variation for T_b and $(T_{out} - T_{in})$ versus airflow and indicates that the temperature variation had an inverse linear relationship with the airflow rate because the heat flow was constant, so any increase in airflow led to a decrease in temperature.

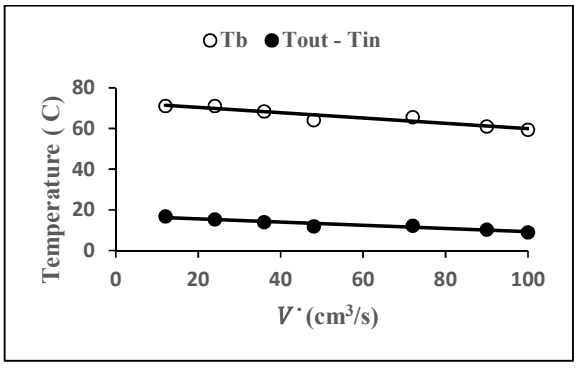

Figure 9 Temperature variation vs $\dot{V}$.

5.1 Exact Solution for Temperature Distribution

In order to obtain the instantaneous distribution of the temperature in the heat sink, a computer program was created using the MATLAB program to simulate Eq. (26) using the parameters τ and N, which were determined from Eqs. (12) and (13) for each volumetric flow rate, as shown in Table 3. Figures 10 to 15 illustrate the transient temperature distribution along the fin length for flow rates 12 to 100 cm^3/s respectively. They indicate that Θ within the fins increased as time progressed because of increasing heat transfer from the base to the fins Θ by conduction, resulting in a decrease in ΔΘ inside the fins and moving the Θ curve upward.

Table 3 Parameters τ and N used in the simulation processes.

$\dot{V}$ cm^3/s	Time s	τ	N	$\dot{V}$ cm^3/s	Time s	τ	N
12	60	0.277	1.201	48	60	0.277	1.2262
	300	1.384	0.8644		300	1.384	0.9006
	600	2.679	0.8267		600	2.679	0.8644
	900	4.153	0.885		900	4.153	0.9688
	1200	5.537	0.969		1200	5.537	1.0779
24	60	0.277	1.1295	72	60	0.277	1.2628
	300	1.384	0.8377		300	1.384	0.9329
	600	2.679	0.7987		600	2.679	0.8980
	900	4.153	0.8267		900	4.153	0.9641
	1200	5.537	0.9450		1200	5.537	1.0587
36	60	0.277	1.1691	100	60	0.277	1.2538
	300	1.384	0.8749		300	1.384	0.9156
	600	2.679	0.8538		600	2.679	0.8607
	900	4.153	0.9131		900	4.153	0.9056
	1200	5.537	1.0884		1200	5.537	1.0413

The level of the Θ curve depends mainly on the N parameter because it is included in a variable characteristic *h*, which is a function of various aspects, such as the geometric, physical, velocity and thermal properties. Observed from previous figures that Θ at the tip of the fin (X = 0) was roughly zero up to the time 60 s because this amount of time was not sufficient to dissipate heat across the fin due to thermal conductivity of the fin material. However, as time progressed, the tip temperature increased and Θ greater than zero was produced, depending on the airflow rate. The influence of the airflow rate was apparent on Θ after 900 s, as Θ_{max} was obtained across the fin at this time at all airflow rates. The reason for this is that the heat transfer coefficient increased with time due to the large temperature differences across the fin. As time advanced after 900 s, the fin approached stability, resulting in lower temperature differences across the fin.

The minimum difference between the 900 and 1200 Θ curves was observed at 12 cm^3/s, while an increase in the airflow rate increased the difference between both until it reached its maximum at 100 cm^3/s. On the other hand, both the 600 and 900 Θ curves were nearly identical at an airflow rate of 48 cm^3/s, indicating that the fin reached a constant temperature for more than half of the fin length from the tip.

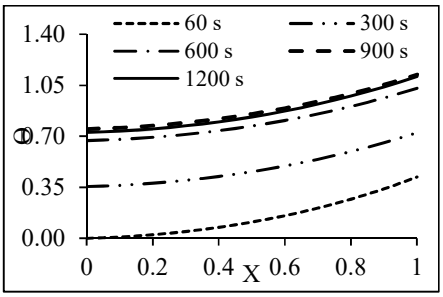

Figure 10 Theoretical transient temperature dimensionless distribution vs X at $\dot{V} = 12cm^2/s$.

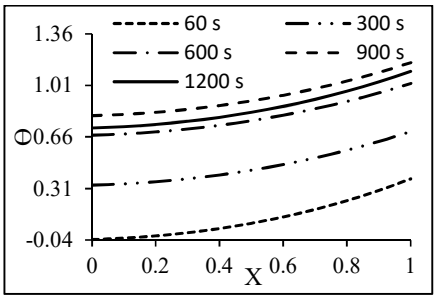

Figure 11 Theoretical transient temperature dimensionless distribution vs X at $\dot{V} = 24\ cm^3/s$.

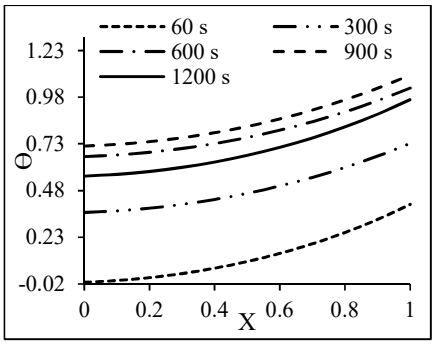

Figure 12 Theoretical transient temperature dimensionless distribution vs X at $\dot{V} = 36\ cm^3/s$.

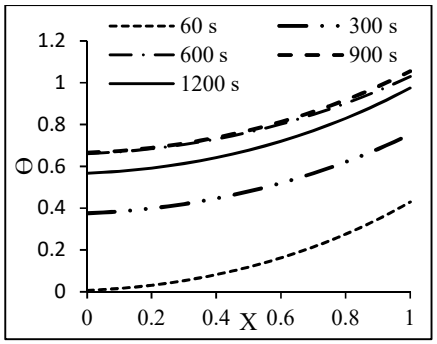

Figure 13 Theoretical transient temperature dimensionless distribution vs X at $\dot{V} = 48\ cm^3/s$.

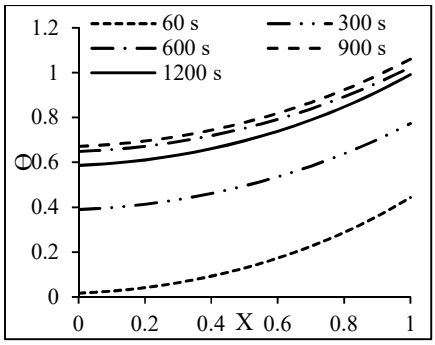

Figure 14 Theoretical transient temperature dimensionless distribution vs X at $\dot{V} = 72\ cm^3/s$.

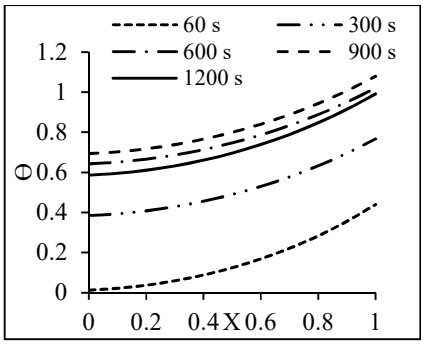

Figure 15 Theoretical transient temperature dimensionless distribution vs X at $\dot{V} = 100\ cm^3/s$.

5.2 Heat Transfer Rate

The exact solution to the transient heat loss was computed based on Eq. 19, which represents the area under the Θ curve at any time of the experiment. To evaluate the transient heat dissipation from the heat sink, which is represented as the region under the dimensionless temperature distribution shown in Figures 10 to 15. The third polynomial arrangement of the curve fitting was used to obtain the equation of the temperature distribution, which is considered the best relationship in this study because $R^2 = 1$ is given. The result of the exact transient solution of the energy losses and the experimental results were plotted for comparison purpuses, as shown in Figures 16 to 21.

A significant similarity was observed in the exact solutions of heat transfer from the heat sink to the flowing air in all experiments, as it was about 70 ± 2 W at 1200 s. The difference in heat transfer in the experiments resulted from the differing working conditions during the experiments. The difference between the experimental heat transfer results was calculated based on the average amount in all airflow rate experiments. They were compared with the exact solution; see Table 5 for the result. It shows that the error rate between the experimental solution and the exact solution increased with an increase in airflow, where the maximum error rate was 6.4% for an airflow rate of 100 cm/s. However, the results of the comparison showed a good match between the two results, and the error rate can be considered acceptable in engineering problems.

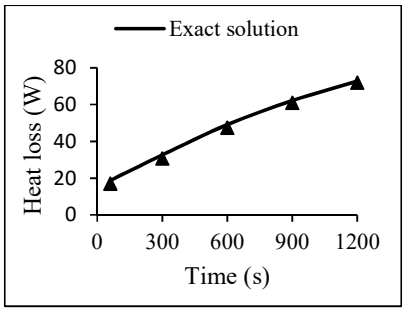

Figure 16 Experimental and theoretical heat loss versus time at $\dot{V} = 12\ cm^3/s$.

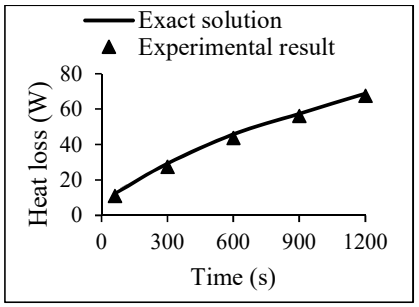

Figure 17 Experimental and theoretical heat loss versus time at $\dot{V} = 24\ cm^3/s$.

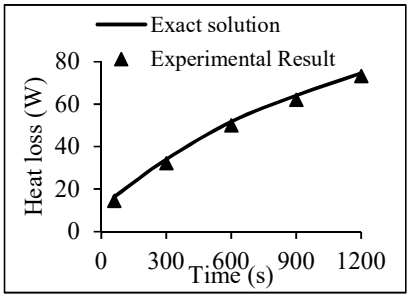

Figure 18 Experimental and theoretical heat loss versus time at $\dot{V} = 36\ cm^3/s$.

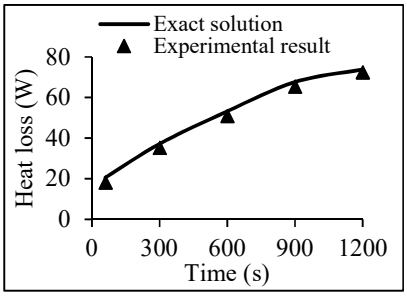

Figure 19 Experimental and theoretical heat loss versus time at $\dot{V} = 48\ cm^3/s$.

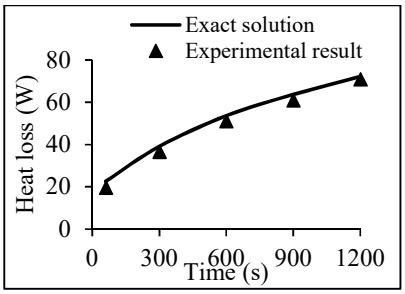

Figure 20 Experimental and theoretical heat loss versus time at $\dot{V} = 72\ cm^3/s$.

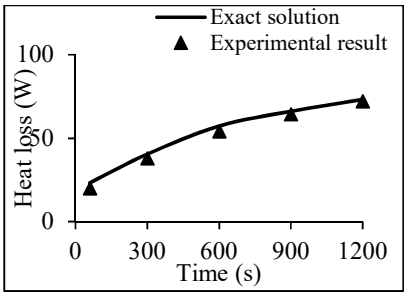

Figure 21 Experimental and theoretical heat loss versus time at $\dot{V} = 100\ cm^3/s$.

Table 4 Average error ratio in the experiments.

Airflow rate cm^3/s	Error ratio %
12	4.1
24	4.7
36	4.9
48	5.2
72	5.8
100	6.4

6 Conclusion

This study compared the exact transient solution of a longitudinal constant cross-section fin and experimental study results in the case of constant heat flux and laminar forced convection. The experiments were conducted at low airflow rate ranges and under nearly identical working conditions. The conclusions of the current study can be summarized as follows:

1. The maximum temperature distribution in the heat sink appeared at the same time (900 s) for all airflow rates.
2. The results showed that the exact transient solution may be applied to predict the preliminary design of heat sinks.
3. The results showed good agreement between the exact solution and the experimental results, and the maximum error ratio did not exceed 6.4%.

Nomenclature

A	Cross section area, m^2
C	Specific heat, J/kg.°C
$\dot{E}$	Change in internal energy
h	Heat transfer coefficient, $W/m^2.°C$
L	Fin length, m
$\dot{m}$	Airflow rate, kg/s
k	Thermal conductivity, W/m.°C
P	Perimeter, m
q	Heat energy, W
q_w	Heat flux W/m^2
t	Fin thickness, m
T	Temperature, °C
U	Uncertainty

Greek symbols

α	Thermal diffusivity, m^2/s
ρ	Density, kg/m^3

Subscripts

a	Air
$conv$	Convection heat transfer
in	Inlet
out	Outlet
∞	Ambient

References

[1] Yeh, R.H. & Chang, M., *Optimum Longitudinal Convective Fin Arrays*, Int. Commun. Heat Mass Transf., **22**(3), pp. 445-460, May 1995.

[2] Sen Kou, H., Lee, J.J. & Lai, C.Y., *Thermal Analysis and Optimum Fin Length of a Heat Sink*, Heat Transf. Eng., **24**(2), pp. 18-29, 2003.
[3] Bar-Cohen, A., Iyengar, M. & Kraus, A.D., *Design of Optimum Plate-fin Natural Convective Heat Sinks*, J. Electron. Packag. Trans. ASME, 2003.
[4] Shih, C.J. & Liu, G.C., *Optimal Design Methodology of Plate-fin Heat Sinks for Electronic Cooling Using Entropy Generation Strategy*, IEEE Trans. Components Packag. Technol., 2004.
[5] Chiang, K.T., *Optimization of the Design Parameters of Parallel-plain Fin Heat Sink Module Cooling Phenomenon Based on the Taguchi Method*, Int. Commun. Heat Mass Transf., 2005.
[6] Chiang, K.T., *Modeling and Optimization of Designing Parameters for a Parallel-plain Fin Heat Sink with Confined Impinging Jet Using the Response Surface Methodology*, Appl. Therm. Eng., **27**(14-15), pp. 2473-2482, Oct. 2007.
[7] Kim, S.M. & Mudawar, I., *Analytical Heat Diffusion Models for Different Micro-channel Heat Sink Cross-sectional Geometries*, Int. J. Heat Mass Transf., **53**(19-20), pp. 4002-4016, Sep. 2010.
[8] Ventola, L., Chiavazzo, E., Calignano, F., Manfredi, D. & Asinari, P., *Heat Transfer Enhancement by Finned Heat Sinks with Micro-structured Roughness*, J. Phys. Conf. Ser., **494**(1), pp. 1-9, 2014.
[9] Raut, S.V. & Kothavale, B.S., *Study on Thermal Performance of Micro Fin Heat Sink under Natural Convection-A Review*, Int. J. Curr. Eng. Technol., **7**(7), pp. 257-261, 2017.
[10] Wu, H.H., Hsiao, Y.Y., Huang, H.S., Tang, P.H. & Chen, S.L., *A Practical Plate-fin Heat Sink Model*, Appl. Therm. Eng., **31**(5), pp. 984-992, 2011.
[11] Lelea, D., *The Heat Transfer and Fluid Flow of a Partially Heated Microchannel Heat Sink*, Int. Commun. Heat Mass Transf., **36**(8), pp. 794-798, Oct. 2009.
[12] Yoon, Y., Park, S.J., Kim, D.R. & Lee, K.S., *Thermal Performance Improvement Based on the Partial Heating Position of a Heat Sink*, Int. J. Heat Mass Transf., **124**, pp. 752-760, Sep. 2018.
[13] Lee, J.J., Kim, H.J. & Kim, D.K., *Experimental Study on Forced Convection Heat Transfer from Plate-fin Heat Sinks with Partial Heating*, Processes, **7**(10), pp. 1-18, 2019.
[14] Gupta, A., Kumar, M. & Patil, A.K., *Enhanced Heat Transfer in Plate Fin Heat Sink with Dimples And Protrusions*, Heat Mass Transf. und Stoffuebertragung, 2019.
[15] Vinoth, R. & Senthil Kumar, D., *Experimental Investigation on Heat Transfer Characteristics of an Oblique Finned Microchannel Heat Sink with Different Channel Cross Sections*, Heat Mass Transf., **54**(12), pp. 3809-3817, 2018.

[16] Rahman, A. & Tafti, D., *Characterization of Heat Transfer Enhancement for an Oscillating Flat Plate-fin*, Int. J. Heat Mass Transf., **147**, 119001, 2020. DOI: 10.1016/j.ijheatmasstransfer.2019.119001.

[17] Yu, Y., Simon, T. & Cui, T., *A Parametric Study of Heat Transfer in an Air-cooled Heat Sink Enhanced by Actuated Plates*, Int. J. Heat Mass Transf., **64**, pp. 792-801, 2013.

[18] Sharath, D., Sathyanarayana, & Puneeth, H.S., *Heat Transfer Numerical Simulation and Optimization of a Heat Sinks*, in IOP Conference Series: Materials Science and Engineering, **376**(1), pp. 1-8, 2018. DOI: 10.1088/1757-899X/376/1/012005

[19] Duan, Z., Lv, X., Ma, H., Su, L. & Zhang, M., *Analysis of Flow Characteristics and Pressure Drop for an Impinging Plate Fin Heat Sink with Elliptic Bottom Profiles*, Appl. Sci., **10**(1), pp. 1-17, 2020. DOI: 10.3390/app10010225.

[20] Ekpu, M., Bhatti, R., Ekere, N., Mallik, S., Amalu, E. & Otiaba, K., *Investigation of Effects of Heat Sinks on Thermal Performance of Microelectronic Package*, 3rd IEEE Int. Conf. Adapt. Sci. Technol. ICAST 2011, Proc., May 2014, pp. 127-132, 2011.

[21] Teertstra, P., Yovanovich, M.M. & Culham, J.R., *Analytical Forced Convection Modeling of Plate Fin Heat Sinks*, J. Electron. Manuf., **10**(4), pp. 253-261, 2000.

[22] Ma, J. & Xu, F., *Transient Flows around a Fin at Different Positions*, in Procedia Engineering, **126**, pp. 393-398, 2015.

[23] Arshad, A., Jabbal, M., Sardari, P.T., Bashir, M.A., Faraji, H. & Yan, Y., *Transient Simulation of Finned Heat Sinks Embedded with PCM for Electronics Cooling*, Therm. Sci. Eng. Prog., **18**, 100520, Aug. 2020.

[24] Panahizadeh, F., Hasnat, M. & Ghafouri, A., *Numerical Modeling of Transient Heat Transfer in Longitudinal Fin*, Analele Universitatii "Eftimie Murgu" Resita. Fascicula de Inginerie, **14**(1), pp. 320-328, 2017.

[25] Lakshminarasimha, N., *Transient CFD Analysis of Different Cross-section Fins Under Free-convection Conditions*, **8**(6), pp. 807-813, 2019.

[26] Naphon, P. & Nakharintr, L., *Turbulent Two Phase Approach Model for the Nanofluids Heat Transfer Analysis Flowing Through the Minichannel Heat Sinks*, Int. J. Heat Mass Transf., **82**, pp. 388-395, 2015.

[27] Naphon, P. & Nakharintr, L., *Numerical Investigation of Laminar Heat Transfer of Nanofluid-cooled Mini-Rectangular Fin Heat Sinks*, J. Eng. Phys. Thermophys., **88**(3), pp. 666-675, 2015.

[28] Nakharintr, L. & Naphon, P., *Magnetic Field Effect on the Enhancement of Nanofluids Heat Transfer of a Confined Jet Impingement in Mini-Channel Heat Sink*, Int. J. Heat Mass Transf., **110**, pp. 753-759, 2017.

[29] Nakharintr, L., Naphon, P. & Wiriyasart, S., *Effect of Jet-plate Spacing to Jet Diameter Ratios on Nanofluids Heat Transfer in a Mini-Channel Heat Sink*, Int. J. Heat Mass Transf., **116**, pp. 352-361, 2018.

[30] Nakharintr, L., Naphon, P. & Wiriyasart, S., *Eulerian Two-Phase Model Analysis on Jet Impingement Nanofluids Heat Transfer in Heat Sinks*, JP J. Heat Mass Transf., **14**(4), 2017.
[31] Naphon, P., Nakharintr, L. & Wiriyasart, S., *Continuous Nanofluids Jet Impingement Heat Transfer and Flow in A Micro-vhannel Heat Sink*, Int. J. Heat Mass Transf., **126**, pp. 924-932, 2018.
[32] Kraus, A.D., Aziz, A. & Welty, J., *Extended Surface Heat Transfer*, New York: John Wiley & Sons, Inc., 2001.
[33] Holman, J.P., *Experimental Methods for Engineering*, 8th ed., McGraw-Hill series in Mechanical Engineering, 2001.
[34] Holman, J.P., *Heat Transfer*, 10th ed., McGraw-Hill series in Mechanical Engineering, 2010.